Coordination Sphere Flexibility of Active-Site Models for Fe-Only Hydrogenase: Studies in Intra- and Intermolecular Diatomic Ligand Exchange

Erica J. Lyon, Irene P. Georgakaki, Joseph H. Reibenspies, and Marcetta Y. Darensbourg*

Contribution from the Department of Chemistry, Texas A&M University, College Station, Texas 77843

Received August 23, 2000. Revised Manuscript Received December 26, 2000

Abstract: A series of dinuclear complexes, (μ-SRS)$Fe_2(CO)_6$ (R = $-CH_2CH_2-$, $-CH_2CH_2CH_2-$, $-CH_2-C_6H_4-CH_2-$; edt, pdt, and *o*-xyldt, respectively) has been examined for specific characteristics that might relate to structural similarity with the active site of Fe-only hydrogenases. Variable-temperature proton NMR studies display the fluxionality of the iron−dithiocyclohexane unit in (μ-pdt)$Fe_2(CO)_6$ while in the (μ-*o*-xyldt)$Fe_2(CO)_6$ compound, the bridge is fixed. Temperature-dependent ^{13}C NMR spectral studies establish intramolecular CO site exchange localized on discrete $Fe(CO)_3$ units in all complexes, which is influenced by steric effects of the μ-SRS unit. Kinetic studies of intermolecular CO/CN^- ligand-exchange reactions establish associative or I_a mechanisms in sequential steps to form the dicyano dianion, (μ-SRS)$[Fe(CO)_2(CN)]_2^=$ with 100% selectivity. Theoretical calculations (DFT) of transition states in the intramolecular site-exchange processes lead to a rationale for the interesting cooperativity in the CN^-/CO intermolecular ligand-exchange process. The hinge motion of the three light atom S-to-S bridge is related to a possible heterolytic H_2 activation/production process in the enzyme.

Introduction

The metabolism of hydrogen is facilitated at a novel 2Fe2S center in Fe-only hydrogenases.[1−3] Recent crystallography reveals that this active site is cysteine-S bridged to a 4Fe4S cluster, the first in a series of iron−sulfur clusters that form the electron-transport route to biological electron donor/acceptor sites. The two irons are further coordinated, bridged together in fact, with two non-protein thiolates or sulfides, and other coordination sites are occupied by diatomic ligands, see Figure 1. With the aid of isotopic labeling experiments, vibrational spectroscopic studies have unambiguously identified ligands with similar spectroscopic signals as CO and CN^- in the binuclear active sites of [NiFe]hydrogenase.[4,5] It is thus assumed that such diatomic ligands, normally incompatible with biology, are pervasive in the active-site architecture of metalloproteins designed for H_2 production or activation.[6]

The [NiFe]H_2ase active sites are securely connected into their respective proteins by multiple cysteines, including two that bridge nickel and iron.[7,8] In contrast, the 2S bridges in Fe-only, or hereafter, [FeFe]H_2ases, while still less than unambiguously defined, are definitely *not* cysteine-S bridges. One study of the active site of [FeFe]H_2ase derived from the 1.6 Å resolution structure of *Desulfovibrio desulfuricans*, DdH, concluded that the S-to-S bridge is composed of three covalently linked light atoms, possibly carbon as in a 1,3-propanedithiolate bridge, (pdt), structure **b)** in Figure 1. Nevertheless, any combination of C, N, or O atoms would satisfy the crystallographic results. The consensus expressed in ref 3a, and amplified in 3b, points out that a heteroatom such as nitrogen or oxygen is an especially good candidate for the central atom of the three-atom linker in that H-bonding from it to S of cysteine 178 in the DdH structure could account for the observed close contact.[1,3]

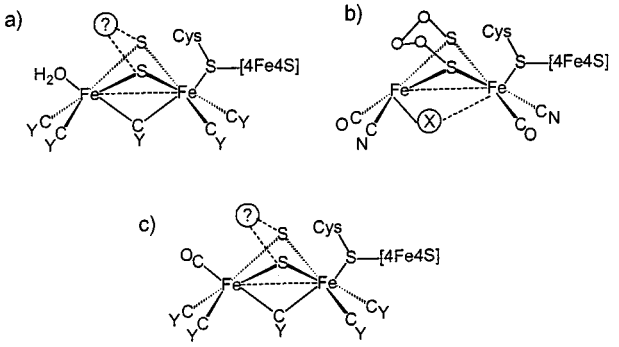

Figure 1. Active sites of [FeFe] H_2ases as determined from protein crystallography: (a) as isolated (oxidized or resting state) from *Clostridium pasteurianum*;[1a] (b) reduced or turnover state from *D. desulfuricans*, X = H_2O;[2] (c) single CO inhibited form of *C. Pasteurianum*.[1b]

(1) (a) Peters, J. W.; Lanzilotta, W. N.; Lemon, B. J.; Seefeldt, L. C. *Science* **1998**, *282*, 1853. (b) Lemon, B. J.; Peters, J. W. *Biochemistry* **1999**, *38*, 12969.

(2) Nicolet, Y.; Piras, C.; Legrand, P.; Hatchikian, C. E.; Fontecilla-Camps, J. C. *Structure* **1999**, *7*, 13.

(3) (a) Nicolet, Y.; Lemon, B. J.; Fontecilla-Camps, J. C.; Peters, J. W. *Trends Biochem. Sci.* **2000** *25*, 138; (b) Nicolet, Y.; de Lacey, A. L.; Vernede, X.; Fernandez, V. M.; Hatchikian, E. C.; Fontecilla-Camps, J. C. *J. Am. Chem. Soc.* **2001**, *123*, 1596.

(4) Happe, R. P.; Roseboom, W.; Pierik, A. J. Albracht, S. P. J.; Bagley, K. A. *Nature* **1997**, *385*, 126.

(5) Bagley, K. A.; Van Garderen, C. J.; Chen, M.; Duin, E. C.; Albracht, S. P. J.; Woodruff W. H. *Biochemistry* **1994**, *33*, 9229.

(6) (a) Pierik, A. J.; Roseboom, W.; Happe, R. P.; Bagley, K. A.; Albracht, S. P. J. *J. Biol. Chem.* **1999**, *274*, 3331. (b) Van der Spek, T. M.; Arendsen, A. F.; Happe, R. P.; Yun, S.; Bagley, K. A.; Stufkens, D. J.; Hagen, W. R.; Albracht, S. P. J. *Eur. J. Biochem.* **1996**, *237*, 629. (c) Pierik, A. J.; Hulstein, M.; Hagen, W. R.; Albracht, S. P. J. *Eur. J. Biochem.* **1998**, *258*, 572.

(7) Frey M. *Struct. Bonding* **1998**, *90*, 97.

(8) Cammack R.; van Vliet, P. In *Bioinorganic Catalysis*, 2nd ed.; Reedijk, J., Ed.; Marcel Dekker: New York, 1999.

10.1021/ja003147z CCC: $20.00
Published on Web 03/17/2001

Scheme 1

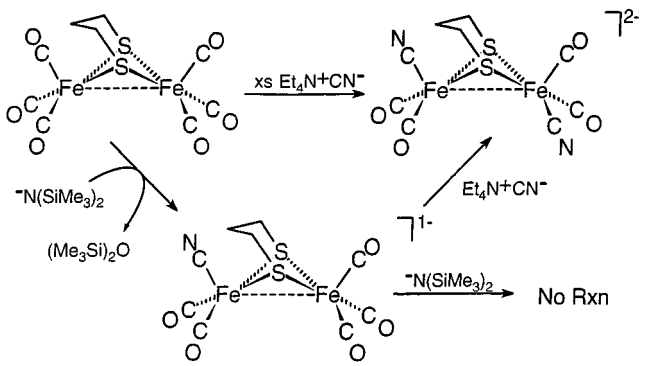

The limited attachment of the dinuclear [FeFe] active site to the protein suggests that it might have been imported into the enzyme as a preconstructed unit.[2] This idea is particularly attractive for the evolution of the catalytic site in that dinuclear iron(I) complexes, $(\mu\text{-SR})_2Fe_2(CO)_6$, form under "primordial" conditions from iron sulfide, alkanethiol, and formic acid, and thus argues for the possibility of their independent existence in prebiotic times.[9] Such complexes, whose rich reactivity was studied extensively by Seyferth et al.,[10] are thus candidates for the evolution of rudimentary mobilized or homogeneous catalysts from inorganic iron sulfides. This view would extend the ideas championed by Wächterhäuser and others regarding the heterogeneous fixation of CO_2 templated on the surface of iron pyrite mineral as the basis for evolutionary biochemistry.[11]

The simple $(\mu\text{-pdt})Fe_2(CO)_6$ complex bears remarkable structural similarities to the active site and can be readily modified by CO/CN^- exchange, Scheme 1.[12] Direct CO/CN^- exchange with a cyanide salt, even with a deficiency of cyanide, results in the dicyano complex $(\mu\text{-pdt})Fe_2(CO)_4(CN)_2^{2-}$.[12,13] The assignment of the structure as drawn in Scheme 1, with one cyanide on each iron atom, was based on changes in the ν(CO) infrared band positions and band intensity pattern as reported earlier.[12] The X-ray crystallographic studies of Rauchfuss, et al., uncovered two of several possible positional isomers.[13] A second route shown in Scheme 1 enlists the $Na^+[N(SiMe_3)_2]^-$ reagent which adds to a single CO, producing an intermediate amido-carbonyl, subsequently releases bis-trimethylsilyl ether, and thereby converts a CO into a CN^-. That this remarkable reaction proceeds through nucleophilic attack is evidenced by the fact that a second equivalent of $(Me_3Si)_2N^-$ will not add to the remaining less electrophilic carbonyl carbons in the anionic monocyano complex.[12] This limited reactivity has been previously observed for reactions of $(Me_3Si)_2N^-$ with $Mn_2(CO)_{10}$.[14] In our case it provides the expected intermediate for direct CN^-/CO exchange.

The dithiolato-bridged dinuclear $(\mu\text{-SR})_2Fe_2(CO)_6$ unit has an extensive organometallic literature regarding Fe- -Fe bond reactivity[15] as well as CO-ligand substitution by phosphines, yielding both mono- and disubstituted phosphine derivatives.[16] Electrophiles, H^+ or SO_2, add into the Fe- -Fe bond density region, while nucleophiles such as PR_3, result in CO displacement via an associative path, with a site preference trans to the Fe- -Fe bond, as shown below. In most of the latter cases, the second substitution reaction is rate-limiting, and production of monosubstituted $(\mu\text{-SR})_2Fe_2(CO)_5L$ complexes is readily controlled by stoichiometry and kinetics.[16] Our work adds to this

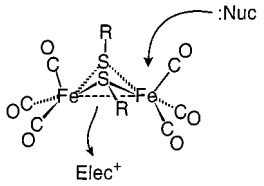

knowledge base in that studies of CN^-/CO substitution even with mononuclear metal carbonyls are rare or nonexistent. In view of the occurrence of mixed ligand sets of $CN^-/CO/SR^-$ within dimetallic complexes in biology, as well as the widespread addition of cyanide and carbon monoxide to metalloproteins as spectroscopic and mechanistic probes (typically as metalloenzyme inhibitors), these studies provide baseline information on reaction rates and on vibrational spectroscopy. We will also attempt to address the role of the unusual linker group between the sulfurs in the active site of hydrogenases. Notably, this class of molecules is configurationally mobile at both the bridging dithiolate as well as at the $Fe(CX)_3$ sites. Variable temperature proton and ^{13}C NMR studies probe site exchanges for possible relationships to reactivity.

Experimental Section

Materials and Techniques. Acetonitrile was distilled once from CaH_2 and once from P_2O_5 and freshly distilled from CaH_2 under N_2 prior to use in kinetic experiments. Toluene, pentane, and THF were purified by distillation under N_2 from sodium/benzophenone. The following materials were of reagent grade and were used as purchased: $Et_4N^+CN^-$, $Fe_3(CO)_{12}$, $LiHBEt_3$, 1,3-propanedithiol, 1,2-ethanedithiol, *o*-xylene−dibromobenzene, $Na^+N(SiMe_3)_2^-$. Kinetic measurements using infrared spectroscopy were carried out using the ReactIR 1000 system from Applied Systems Inc., equipped with a MCT detector and 30 bounce SiCOMP in situ probe. For reactions monitored by UV/vis spectroscopy, a Hewlett-Packard 8453 spectrophotometer was employed which was equipped with a multicell transport that can be attached to a controlled temperature bath. ^1H- and ^{13}C NMR spectra were recorded on a Unity+ 300 MHz superconducting NMR instrument equipped with a variable-temperature control module and operating at 299.9 and 75.43 MHz, respectively. All spectra were referenced using published solvent resonances.

Preparations. The known diiron hexacarbonyl compounds used in the following studies were prepared by refluxing toluene solutions of the appropriate thiol or dithiol (typically, ~1 mL, 8 mmol) with $Fe_3(CO)_{12}$ (typically, ~4 g, 8 mmol in 20 mL toluene), under N_2, until a color change from green to red−brown was observed.[17] Following

(9) Cody, G. D.; Boctor, N. Z.; Filley, T. R.; Hazen, R. M.; Scott, J. H.; Sharma, A.; Yoder Jr., H. S. *Science* **2000**, *289*, 1337.

(10) (a) Seyferth, D.; Henderson, R. S.; Song, L.-C. *Organometallics* **1982**, *1*, 125. (b) Seyferth, D.; Womack, G. B.; Song, L.-C. *Organometallics* **1983**, *2*, 776. (c) Seyferth, D.; Song, L.-C.; Henderson, R. S. *J. Am. Chem. Soc.* **1981**, *103*, 5103. (d) Messelhauser, J.; Gutensohn, K. U.; Lorenz, I.-P.; Hiller, W. *J. Organomet. Chem.* **1987**, *321*, 377.

(11) (a) Wächterhäuser, G. *Prog. Biophys. Mol. Biol.* **1992**, *58*, 85; (b) Pontes-Buarque, M.; Tessis, A. C.; Bonapace, J. A. P.; Monte, M. B. M.; de Souza-Barros, F.; Vieyra, A. *An. Acad. Bras. Cienc.* **2000**, *72*, 317.

(12) Lyon, E. J.; Georgakaki, I. P.; Reibenspies, J. H.; Darensbourg, M. Y. *Angew. Chem., Int. Ed.* **1999**, *38*, 3178.

(13) (a) Schmidt, M.; Contakes, S. M.; Rauchfuss, T. B. *J. Am. Chem. Soc.* **1999**, *121*, 9736. (b) Schmidt, M.; Contakes, S. M.; Rauchfuss, T. B. *Abstract from the 218th ACS National Meeting*, **1999**.

(14) Behrens H.; Moll, M.; Popp W.; Würstl, P. *Z. Naturforsch.* **1977**, *32b*, 1227.

(15) (a) Treichel, P. M.; Rublein, E. K. *J. Organomet. Chem.* **1989**, *359*, 195. (b) Arabi, M. S.; Mathieu, R.; Poilblanc, R. *J. Organomet. Chem.* **1979**, *177*, 199. (c) Arabi, M. S.; Mathieu, R.; Poilblanc, R. *Inorg. Chim. Acta* **1979**, *34*, L207. (d) Arabi, M. S.; Mathieu, R.; Poilblanc, R. *Inorg. Chim. Acta* **1977**, *23*, L17.

(16) (a) Maresca, L.; Greggio, F.; Sbrignadello, G.; Bor, G. *Inorg. Chim. Acta* **1971**, 667. (b) Basato, M. *J. Chem. Soc., Dalton Trans.* **1975**, 911. (c) Aime, S.; Gervasio, G.; Rossetti, R.; Stanghellini, P. L. *Inorg. Chim. Acta* **1980**, *40*, 131. (d) Ellegan, P. C.; Gerlach, J. N. *Inorg. Chem.* **1973**, *12*, 2526.

solvent reduction to a few mL, the products were purified by chromatography on successive silica columns (1 in. × 12 in.), the first with toluene as eluant followed by pentane. Crystalline products were obtained by cooling the concentrated pentane solutions at −20 °C overnight. Average yield: 3−4 mmol. Spectroscopic data: (μ-SCH_2-CH_2CH_2S)$Fe_2(CO)_6$: ^{1}H NMR (acetone-d_6) 2.26 (t, 4H), 1.86 (m, 2H); ^{13}C NMR 208.9, 31.2, 23.6 ppm; ν(CO) CH_3CN, 2072(m), 2033(s), 1992(s br) cm^{-1}; absorption spectra (λ_{max}) 327(13000), 459(1100) nm. (μ-SCH_2CH_2S)$Fe_2(CO)_6$: ^{1}H NMR ($CDCl_3$) 2.39(t) ppm; ^{13}C NMR 208.9, 36.5 ppm; ν(CO) CH_3CN, 2078(m), 2037(s), 1997(s br) cm^{-1}; absorption spectra (λ_{max}) 323(12000), 448(1000) nm.

Synthesis of (μ-$SCH_2C_6H_4CH_2S$)$Fe_2(CO)_6$.[18] To the red solution of (μ-S_2)$Fe_2(CO)_6$ (0.985 g, 2.86 mmol) in THF (30 mL) at −78 °C was added $LiHBEt_3$ (5.7 mL of 1 M in THF, 5.7 mmol); the color changed immediately to dark green. A solution of α,α′-dibromo-*o*-xylene (0.77 g, 2.91 mmol) in THF (15 mL) at ambient temperature was then added. The reaction mixture was stirred for 5−6 h while slowly warming up to room temperature, giving rise to a red solution. Following solvent reduction in vacuo, the product was purified by column chromatography, silica/THF, followed by a second column, silica/pentane. The red−orange product crystallized from a concentrated, cooled pentane solution. ^{1}H NMR (300 MHz, CD_3CN): 7.14 (m, 4H), 3.96 (d, 2H), 3.25 ppm (d, 2H); IR (in CH_3CN, cm^{-1}): 2072(m), 2037(s), 1996(s br).

(μ-$SCH_2CH_2CH_2S$)$Fe_2(CO)_5(CN)^-$ and (μ-$SCH_2C_6H_4CH_2S$)$Fe_2(CO)_5(CN)^-$. Cannula transfer of (μ-$SCH_2CH_2CH_2S$)$Fe_2(CO)_6$ (0.25 g, 0.65 mmol, dissolved in 8 mL of THF) to a solution of $Na^+N(SiMe_3)_2^-$ (0.11 g, 0.60 mmol, in 8 mL of THF) resulted in a red−brown solution which was magnetically stirred for 1 h. After solvent removal, the resulting red−black oil was triturated six times with 15−20 mL portions of dry degassed pentane. The dried solid may be stored for no more than a few days at 22° under inert atmosphere. Yield, ∼75%. ^{1}H NMR (CD_3CN): 2.17 (t, 4H), 1.77 ppm (m, 2H); IR in THF ν(CN); 2103(w) ν(CO) 2027(s), 1977(s), 1944(vs), 1919(s br) cm^{-1}; absorption spectra (in CH_3CN, λ_{max}) 344(7,900) nm. The *o*-xylenedithiolate derivative was prepared similarly: IR (in THF, cm^{-1}), ν(CN); 2102 (w) ν(CO) 2029(s), 1985(s), 1948(vs), 1924(s br).

Kinetic Measurements. Pseudo-first-order reaction conditions were employed for all kinetic studies, using 20-fold and greater excesses of $Et_4N^+CN^-$. Reactions were monitored by vibrational and electronic spectroscopies. For the former, kinetic studies were carried out in a reaction vessel designed to contain the in situ IR probe (ReactIR). The cell was degassed through a sidearm fitted with a rubber septum. Typically 12 mL of an CH_3CN solution containing the iron dimetallic was introduced, and the cell was placed in a temperature-controlled bath. Following temperature equilibration, ∼2 mL of an CH_3CN solution of $Et_4N^+CN^-$ was added via syringe. While being magnetically stirred, IR spectra were taken every 30 s typically through seven half-lives. The probe and vessel were periodically shaken to expel CO which collected on the surface of the crystal probe. Rates of reaction were measured by following the decrease in absorption of the reactants' most intense ν(CO) vibration, which centered around 2038 cm^{-1} for the μ-pdt and μ-edt derivatives, and an intermediate band at 1978 cm^{-1} for μ-*o*-xyldt. Kinetic studies using UV/vis spectroscopy were done using a multicell transport and two cuvettes. The first cuvette, a blank, was filled with 2.5 mL of CH_3CN. The second cuvette was filled with 2.5 mL of CH_3CN and a 50 μL aliquot of the appropriate diiron stock solution. The reaction monitor was initiated as the cyanide solution was added. The reactions were followed to completion, typically accumulating 60 full spectra (200−1100 nm). The reaction rate was determined from the disappearance of reactant absorbance at ∼325 nm. Rate constants were calculated from first-order rate plots of $\ln(A_t - A_\infty)$ versus time; activation parameters were obtained from Eyring plots.

X-ray Crystal Structure. The X-ray crystal structure of (μ-$SCH_2C_6H_4CH_2S$)$Fe_2(CO)_6$. was solved at the Crystal & Molecular Structure Laboratory Center for Chemical Characterization and Analysis at Texas A&M University. X-ray crystallographic data were obtained on a Bruker SMART 1000 three-circle diffractometer operating at 50 kV and 40 mA, Mo Kα (λ = 0.71073 Å) with a graphite monochromator and a CCD-PXL-KAF2 detector. Diffractometer control software SMART 5.059 and data reduction software SAINTPLUS were supplied by Bruker Analytical X-ray Systems.[19] All crystallographic calculations were performed with use of the SHELXTL-PLUS program package.[20] The structure was solved by direct methods. Anisotropic refinement for all non-hydrogen atoms was done by a full-matrix least-squares method. A single crystal was mounted on a glass fiber with epoxy cement at 110 K in a N_2 cold stream. Crystals are triclinic, space group, $P\bar{1}$, with a = 7.5881(9) Å, b = 9.8125(12) Å, c = 12.3687(14) Å, α = 72.345(2)°, B = 73.037(2)°, γ = 70.665(2)°, and Z = 2, R = 0.0390 and R' = 0.0402 for 4860 reflections.

Computational Details. Full geometry optimizations utilized ab initio calculations for the nonmetal systems (MP2/6-31G) and density functional theory (DFT) for the iron- and thiolate-containing complexes. Becke three-parameter hybrid exchange functional[21] and LYP correlation functional[22] (B3LYP) were used in the DFT calculations. Symmetry, C_s or C_{2v}, was imposed on the structures submitted for DFT geometry optimizations. All calculations were performed using the Gaussian 98 programs[23] at the Laboratory for Molecular Simulation at Texas A&M University on an SGI Powerchallenge computer with a Silicon Graphic Indigo2 workstation.

Calculations with C, H, and O atoms used a Dunning basis set of double-ζ quality.[24] A modified version of the Hay and Wadt double-ζ basis set with effective core potentials (ECP)[25] was used for the Fe atoms and taken from the work of Couty and Hall.[26] A polarization function optimized for the double-ζ basis set and ECPs of Hay and Wadt[25] were used for the sulfur atoms in accordance to the work of Höllwarth, et al.[27]

Results and Discussion

Effects of S-to-S Links: Structures of Model Compounds. To examine effects of the S-to-S bridge on CN^-/CO ligand exchange, the more constrained ethanedithiolate (edt), (μ-

(17) Winter, A.; Zsolnai, L.; Huttner, G. *Z. Naturforsch.* **1982**, *37b*, 1430.

(18) Seyferth, D.; Womack, G. B.; Gallagher, M. K.; Cowie, M.; Hames, B. W.; Fackler, J. P., Jr.; Mazany, A. M. *Organometallics* **1987**, *6*, 283.

(19) *SMART*, ver. 5.059; Bruker Analytical X-ray Systems: Madison, WI, 1999.

(20) (a) *SAINT-Plus*, vers. 6.02; Bruker: Madison, WI, 1999. (b) Sheldrick, G. *SHELXS-86*, Program for Crystal Structure Solution; Institut fur Anorganische Chemie der Universitat: Gottingen, Germany, 1986. (c) Sheldrick, G. *SHELXL-97*, Program for Crystal Structure Refinemen; Institut fur Anorganische Chemie der Universitat: Gottingen, Germany, 1997. (d) *SHELXTL*, vers. 5.0; Bruker: Madison, WI, 1999.

(21) (a) Becke, A. D. *Phys. Rev. A.* **1988**, *38*, 3098. (b) Becke, A. D. *J. Chem. Phys.* **1993**, *98*, 1372. (c) Becke, A. D. *J. Chem. Phys.* **1993**, *98*, 5648.

(22) (a) Lee, C.; Yang, W.; Parr, R. G. *Phys. Rev. B* **1988**, *37*, 785. (b) Miehlich, B.; Savin, A.; Stoll, H.; Preuss, H. *Chem. Phys. Lett.* **1989**, *157*, 200.

(23) Frisch, M. J.; Trucks, G. W.; Schlegel, H. B.; Scuseria, G. E.; Robb, M. A.; Cheeseman, J. R.; Zakrzewski, V. G., Jr.; Stratmann, R. E.; Burant, J. C.; Dapprich, S.; Millam, J. M.; Daniels, A. D.; Kudin, K. N.; Strain, M. C.; Farkas, O,; Tomasi, J.; Barone, V.; Cossi, M.; Cammi, R.; Mennucci, B.; Pomelli, C.; Adamo, C.; Clifford, S.; Ochterski, J.; Petersson, G. A.; Ayala, P. Y.; Cui, Q.; Morokuma, K.; Malick, D. K.; Rabuck, A. D.; Raghavachari, K.; Foresman, J. B.; Cioslowski, J.; Ortiz, J. V.; Stefanov, B. B.; Liu, G.; Liashenko, A.; Piskorz, P.; Komaromi, I.; Gomperts, R.; Martin, R. L.; Fox, D. J.; Keith, T.; Al-Laham, M. A.; Peng, C. Y.; Nanayakkara, A.; Gonzalez, C.; Challacombe, M.; Gill, P. M. W.; Johnson, B.; Chen, W.; Wong, M. W.; Andres, J. L.; Gonzalez, C.; Head-Gordon, M.; Replogle, E. S.; Pople, J. A.; *Gaussian 98*, revision A.4; Gaussian, Inc.: Pittsburgh, PA, 1998.

(24) (a) Dunning, T. H., Jr. *J. Chem. Phys.* **1970**, *53*, 2823. (b) Dunning, T. H., Jr.; Hay, P. J. *Modern Theoretical Chemistry*; Plenum: New York, 1976; pp 1−28.

(25) (a) Hay, P. J.; Wadt, W. R. *J. Chem. Phys.* **1985**, *82*, 270. (b) Hay, P. J.; Wadt, W. R. *J. Chem. Phys.* **1985**, *82*, 284. (c) Hay, P. J.; Wadt, W. R. *J. Chem. Phys.* **1985**, *82*, 299.

(26) Couty, M.; Hall, M. B. *J. Comput. Chem.* **1996**, *17*, 1359.

(27) Höllwarth, A.; Böhme, M.; Dapprich, S.; Ehlers, A. W.; Gobbi, A.; Jonas, V.; Köhler, K. F.; Stegmann, R.; Veldkamp, A.; Frenking, G. *Chem. Phys. Lett.* **1993**, *208*, 237.

Table 1. Acetonitrile Solution IR Spectra (ν(CO) and ν(CN) Region) for (μ-S−R−S)$Fe_2(CO)_6$ and Product ($[Et_4N^+]_2[(\mu$-S−R−S)$Fe_2(CO)_4(CN)_2^{2-}]$); Rate Data for Reaction with 20-fold Excess $Et_4N^+CN^-$ in CH_3CN Solution at −8 °C[a]

compound [b] (μ-SR)$_x$$Fe_2(CO)_6$	ν(CO) reactants, cm^{-1} m, vs, s	**ν(CN)**, ν(CO) products, cm^{-1}	k_2, M^{-1} s^{-1} [c]
(μ-$SCH_2CH_2CH_2S$)	2074, 2036, 1995	**2076**	8.69×10^{-3}
		1964, 1924, 1885	
(μ-SCH_2CH_2S)	2078, 2038, 1997	**2078**	5.57×10^{-3}
		1966, 1924, 1887	
(μ-$SCH_2C_6H_4CH_2S$)	2076, 2040, 1999	**2074**	$\sim 13 \times 10^{-2}$
		1966, 1930, 1891	
			$\sim 2.4 \times 10^{-3}$

[a] Rate data measured by monitoring ν(CO) $\cong$ 2036−2040 cm^{-1} for μ-pdt and μ-edt and ν(CO) $\cong$ 1978 cm^{-1} for μ-*o*-xyldt. [b] $[Fe_2] \approx 0.010$ M; $[CN^-] \approx 0.192$ M for all. [c] k_2 reported: for μ-pdt and μ-edt, the first CN^-/CO substitution rate limiting; for μ-*o*-xyldt, both the first (k_2) and the second (k_2') second-order rate constants for CN^-/CO substitution were determined.

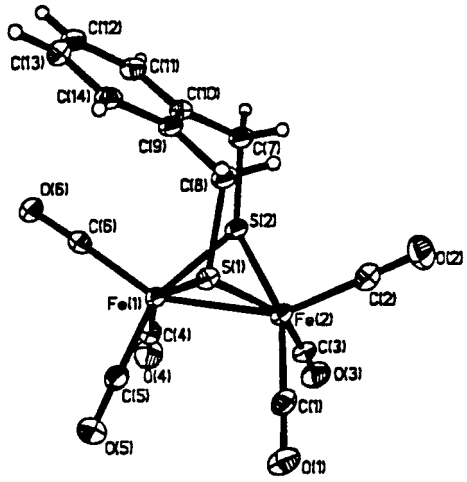

Figure 2. Molecular structure of (μ-SCH_2−C_6H_4−CH_2S)$Fe_2(CO)_6$ (ORTEP plot, thermal elipsoids at 50% probability). Selected bond lengths and angles given in Table 2.

$SCH_2CH_2S)Fe_2(CO)_6$, as well as the less rigid *o*-xylylenedithiolate, (*o*-xyldt), derivative, (μ-$SCH_2C_6H_4CH_2S$)$Fe_2(CO)_6$, was compared to the (presumably) biologically relevant propanedithiolate, pdt, bridged complex, (μ-$SCH_2CH_2CH_2S$)$Fe_2(CO)_6$. The similarity in ν(CO) values, Table 1, indicates that the donor abilities of the three bridging dithiolates are substantially the same. All compounds readily react with $Et_4N^+CN^-$ to yield dicyano products in which each iron is ligated with two carbonyls and one cyanide. Table 1 lists the ν(CO) and ν(CN) values of the final dicyano product of CN^-/CO exchange with (μ-SRS)$Fe_2(CO)_6$. These also show no significant trends in electronic effects.

The (μ-$SCH_2C_6H_4CH_2S$)$Fe_2(CO)_6$ compound, hereafter (μ-*o*-xyldt)$Fe_2(CO)_6$, reported by Seyferth, et al., in 1987,[18] was subjected to X-ray crystal structure analysis. Its molecular structure, shown in Figure 2, is typical of this class of compounds. The iron atoms are in pseudo-square-pyramidal coordination geometry, with thiolate S atoms in the edge-bridged basal planes. There is a displacement of Fe atoms out of the best planes fitted to the $S_2C(ba)_2$ and toward the apical CO by 0.4122 Å (Fe(1)) and 0.4001 Å (Fe(2)). The Fe- -Fe distance of 2.5067(5) Å, Table 2, is consistent with the metal−metal bond required to satisfy the 18-electron count, and compares well to the Fe- -Fe distance in [FeFe]H_2ases of 2.6 Å. The (μ-*o*-xyldt)Fe_2 unit creates two fused seven-membered rings, iron−dithio-*o*-xylene, analogous to the chair and boat conformers in the fused iron−dithiocyclohexane rings of (μ-pdt)$Fe_2(CO)_6$. In the boat form of (μ-*o*-xyldt)$Fe_2(CO)_6$, the arene group of the *o*-xylene lies close and parallel to one of the apical carbonyls with an average CO vector to C_6-plane distance of 3.12 Å. The average S−C−C angle that determines this bend-over of the *o*-xyldt group is 114.5°, ∼5° less than the analogous angle seen in the propane−dithiolate bridge, 118.9°. [Disorder in the bridgehead carbon of the latter actually renders that value suspect. Nevertheless, even if artificially large, the distances of bridgehead methylene-hydrogen to C and to O of the adjacent carbonyl group are 2.712 and 2.896 Å, respectively.]

Table 2. Selected Bond Lengths [Å] and Angles [deg] for (μ-*o*-xyldt)$Fe_2(CO)_6$

Bond Lengths		Bond Angles	
Fe(1)−Fe(2)	2.5067(5)	S(2)−Fe(1)−S(1)	87.20(2)
Fe(1)−S(1)	2.2653(7)	Fe(1)−S(1)−Fe(2)	67.31(2)
Fe(1)−S(2)	2.2600(7)	Fe(1)−S(2)−Fe(2)	67.09(2)
S(2)−C(7)	1.853(2)	C(9)−C(8)−S(1)	113.02(16)
S(1)−C(8)	1.841(2)	C(10)−C(7)−S(2)	116.10(17)
C(8)−C(9)	1.502(3)	C(5)−Fe(1)−C(4)	91.75(12)
C(7)−C(10)	1.501(3)	C(5)−Fe(1)−C(6)	99.12(11)
Fe(1)−C(6)	1.819(3)	C(4)−Fe(1)−C(6)	99.08(11)
Fe(1)−C(5)	1.798(3)	C(5)−Fe(1)−S(2)	157.36(8)
Fe(1)−C(4)	1.797(3)	C(4)−Fe(1)−S(2)	85.87(8)
O(6)−C(6)	1.142(3)	C(6)−Fe(1)−S(2)	103.49(8)
O(5)−C(5)	1.138(3)	C(6)−Fe(1)−S(1)	106.13(8)
O(4)−C(4)	1.139(3)		

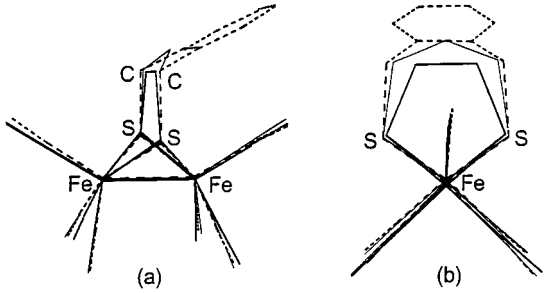

Figure 3. Overlay of three structures represented as line drawings (a) a side-on view; (b) end-on view.

"Side-on" views of the structural differences of (μ-*o*-xyldt)$Fe_2(CO)_6$, (μ-pdt)$Fe_2(CO)_6$, and (μ-edt)$Fe_2(CO)_6$ are seen in the overlays of the three structures given in Figure 3a. Only minor differences are observed in the $Fe_2(CO)_6$ portion of the structure; however, the constraints of the edt bridge in (μ-SCH_2CH_2S)$Fe_2(CO)_6$, result in a shorter S-to-S distance, 2.886 Å, and a significantly smaller S−Fe−S angle (av 80.2°)[28] as compared to the other members of this series: ((μ-pdt)$Fe_2(CO)_6$, S···S = 3.050 Å and S−Fe−S = 85.3°; (μ-*o*-xyldt)$Fe_2(CO)_6$, 3.121 Å and 87.2°), Figure 3b. The S···S distances of >3.0 Å in the model complexes compare well with those in the enzyme structures (3.152 Å for Ddh).[1−3] The dihedral angles defined by the intersection of the FeS_2 and C_2S_2 planes, see Figure 3, are in the range of 129−133.5°. As noted earlier, with exception of the third bridging ligand, the 2Fe2S cores of the organometallic models and the enzyme active sites, are excellent structural matches.

Kinetic Studies of CN^-/CO Exchange into (μ-pdt)$Fe_2(CO)_6$. Reactions of (μ-pdt)$Fe_2(CO)_6$ with $Et_4N^+CN^-$ to yield (μ-pdt)$Fe_2(CO)_4(CN)_2^{2-}$, eq 1, were carried out in CH_3CN solution, under pseudo-first-order conditions of 20-fold and greater excesses of $Et_4N^+CN^-$.

(28) (a) Messelhauser, J.; Lorenz, I. P.; Haug, K.; Hiller, W. *Z. Naturforsch.* **1985**, *40B*, 1064. (b) Hughes, D. L.; Leigh, G. J.; Paulson, D. R. *Inorg. Chim. Acta* **1986**, *120*, 191.

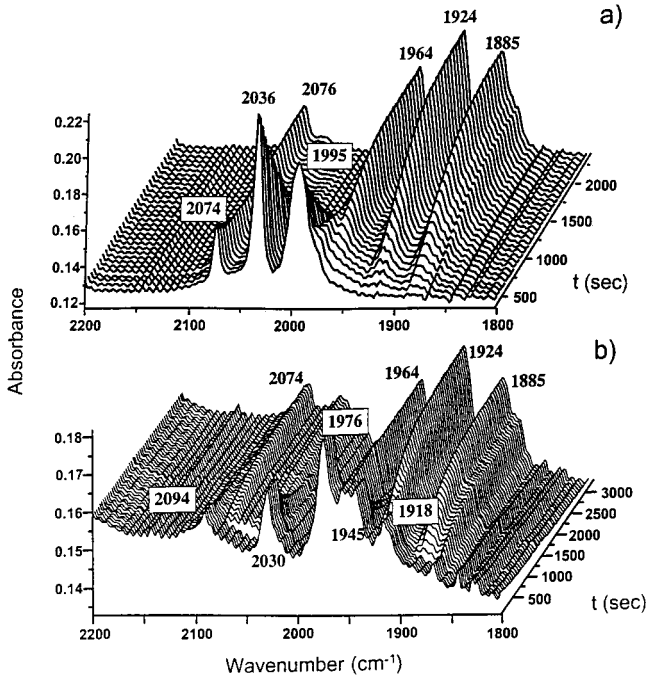

Figure 4. Infrared spectra, in the 1800−2200 cm^{-1} region, as CO/CN^- exchange takes place to produce (μ-pdt)$Fe_2(CO)_4(CN)_2^{2-}$ from (a) (μ-pdt)$Fe_2(CO)_6$ and (b) (μ-pdt)$Fe_2(CO)_5(CN)^-$.

$$(\mu\text{-pdt})\text{-}Fe_2(CO)_6 + \text{xs}\ Et_4NCN \xrightarrow{CH_3CN} (\mu\text{-pdt})Fe_2(CO)_4(CN)_2^{2-} \quad (1)$$

$$\text{Rate} = k_2[(\mu\text{-pdt})Fe_2(CO)_6][CN^-] \quad (2)$$

Figure 4a presents stacked plots of infrared spectra in the 2000 cm^{-1} region which illustrate the rate data obtained for this reaction by use of the in situ ReactIR probe. Kinetic parameters for the reaction of (μ-pdt)$Fe_2(CO)_6$ with $Et_4N^+CN^-$ were determined by monitoring the disappearance of the ν(CO) band at 2036 cm^{-1} with time. The appearance of product band at 1885 cm^{-1} yielded similar results with better reliability at lower temperatures. The data measured at −8 °C were used to determine the rate expression; plots of $\ln(A_t - A_\infty)$ vs time showed good linearity over 3−5 half-lives, Figure 5. Thus-derived values of k_{obs} at various cyanide concentrations, as determined by infrared spectroscopy, are given in Table 3, entries 1−7. Each k_{obs} was obtained from a single kinetic run, with ∼40 spectral accumulations per run. Compounds used for the entries in Table 3 were from four different syntheses and isolations.

Kinetic data for this reaction were also obtained using UV/vis spectroscopy; derived rate data are similar to those obtained by IR spectroscopy. As shown in Figure 6, the absorbance at 327 nm for the starting material decreases as the 355 nm absorbance, due to the disubstituted product, grows in. Several isobestic points are observed. Derived rate constants are given as entries 8−10 in Table 3. The use of IR and UV/vis techniques in tandem permits measurement of k_{obs} over a ∼30-fold cyanide concentration range. The plot of $\ln(k_{obs})$ vs $\ln[CN^-]$, using a combination of IR and UV data, shows good linearity, Figure 7, and has a slope of 0.93 indicating the rate determining step for the overall reaction follows a second-order rate expression, eq 2.

An ill-defined shoulder on the 1995 cm^{-1} IR band of (μ-pdt)$Fe_2(CO)_6$ is seen in the stacked plots of the overall reaction of (μ-pdt)$Fe_2(CO)_6$ with $Et_4N^+CN^-$, Figure 4a. While this band corresponds to the major absorbance of the monocyano species, [(μ-pdt)$Fe_2(CO)_5(CN)]^-$, the expected intermediate of a single CN^-/CO exchange, vide infra, it did not build up to any

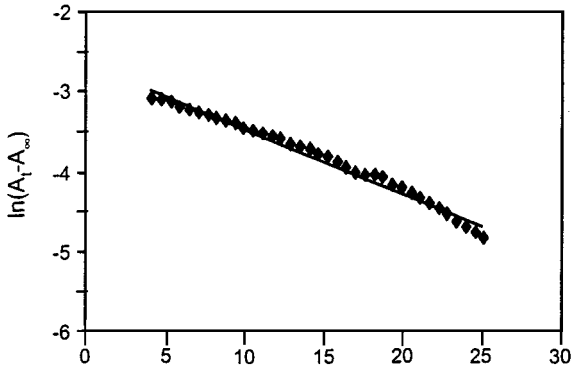

Figure 5. Example plot of $\ln(A_t - A_\infty)$ vs time over four half-lives, Entry 4, Table 3.

Table 3. Rate Data for the Reaction of $Et_4N^+CN^-$ with (μ-pdt)$Fe_2(CO)_6$ (**1**) and with[Na^+][(μ-pdt)$Fe_2(CO)_5(CN)^-$] (**2**) in CH_3CN Solution Measured at −8 °C

entry	compd	[CN^-], M	10^3 k_{obs}, sec^{-1}
1	**1**[a]	0.094	0.96
2	**1**	0.105	1.02
3	**1**	0.135	1.24
4	**1**	0.142	1.42
5	**1**	0.168	1.82
6	**1**	0.184	1.66
7	**1**	0.202	2.42
8	**1**	0.0075	0.08
9	**1**	0.0242	0.40
10	**1**	0.0869	1.1
	av $k_2 = 11.1\ (\pm 2.2) \times 10^{-3}\ M^{-1}\ sec^{-1}$		
11	**2**[b]	0.113	2.67
12	**2**	0.148	3.03
13	**2**	0.148	2.75
14	**2**	0.192	4.83
15	**2**	0.240	5.56
	av $k_2 = 22.2\ (\pm 2.6) \times 10^{-3}\ M^{-1}\ s^{-1}$		

[a] $[Fe_2] = 2.6-8.7 \times 10^{-3}$ M with 20−40-fold excess CN^-. [b] $[Fe_2] = 5.5-8.2 \times 10^{-3}$ M with 20−40-fold excess CN^-.

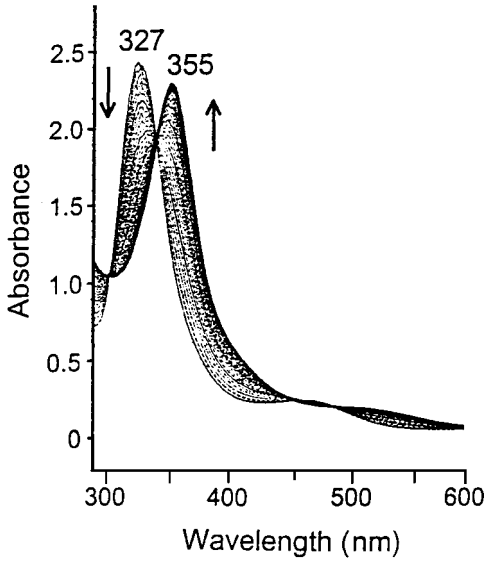

Figure 6. UV/vis spectral monitor of the reaction of (μ-pdt)$Fe_2(CO)_6$, (major band decreasing at 327 nm) with $Et_4N^+CN^-$, producing (μ-pdt)$Fe_2(CO)_4(CN)_2^{2-}$, (major band increasing at 355 nm) in CH_3CN solution.

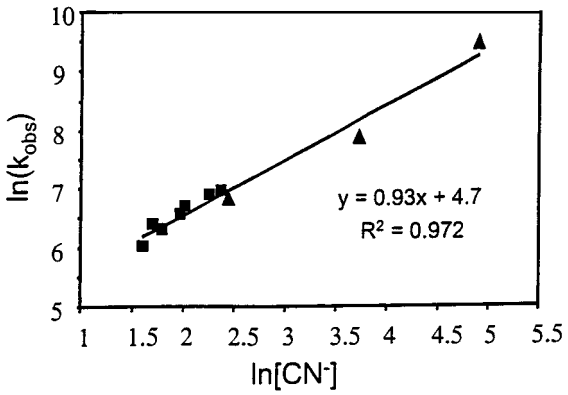

Figure 7. Plot of $\ln(k_{obs})$ vs $\ln[CN^-]$ includes rate data from both vibrational (■) and electronic (▲) spectroscopies at −8 °C.

appreciable extent. To test the competency of $[(\mu\text{-pdt})Fe_2(CO)_5(CN)]^-$ as a kinetic intermediate, a sample of the anion was prepared according to the synthetic approach of CO conversion to CN^- by use of the $Na^+[N(SiMe_3)_2]^-$ reagent, Scheme 1. The light-brown solid thus obtained is air-sensitive, soluble in THF and CH_3CN, and extremely hygroscopic. Its spectral properties are consistent with the monocyano anion shown in Scheme 1.[12] Its thermodynamic stability is limited even in the solid state. On storage under argon inside the glovebox (22 °C), it decomposes into the parent $(\mu\text{-pdt})Fe_2(CO)_6$ and insoluble solids. Consistent with earlier reports of the selective addition of only one equivalent of the silyl amide reagent to $Mn_2(CO)_{10}$,[14] even 20-fold excesses of $Na^+[N(SiMe_3)_2]^-$ do not induce further reaction with $[(\mu\text{-pdt})Fe_2(CO)_5(CN)]^-$. Nevertheless, the latter readily reacts with $Et_4N^+CN^-$ even at low temperatures to yield the same dicyano complex as recovered from the overall reaction of $Et_4N^+CN^-$ with $(\mu\text{-pdt})Fe_2(CO)_6$.

The reaction of Na^+ $[(\mu\text{-pdt})Fe_2(CO)_5(CN)]^-$ with $Et_4N^+CN^-$ in CH_3CN solution, eq 3, was monitored by IR, under pseudo-first-order conditions of 20-fold and larger excesses of cyanide; sample stacked plots are shown in Figure 4b. The disappearance of the band at 1976 cm^{-1} showed linearity in the ln[Abs] versus time plot, as well as a first-order dependence on $[CN^-]$, eq 4. The rate constants derived, entries 11−15 in Table 3, are about twice larger than those obtained from the $(\mu\text{-pdt})Fe_2(CO)_6/CN^-$ reaction.

$$(\mu\text{-pdt})Fe_2(CO)_5(CN)^- + \text{xs } Et_4CN \xrightarrow{CH_3CN} (\mu\text{-pdt})Fe_2(CO)_4(CN)_2^{2-} \quad (3)$$

$$\text{Rate} = k_2'[(\mu\text{-pdt})Fe_2(CO)_5(CN)^-][CN^-] \quad (4)$$

Control Experiments. A question is whether the increase in rate of CN^-/CO exchange in the reaction described by eq 3, entries 11−15 in Table 3, as compared to the eq 1 reaction, entries 1−10, could result from counterion differences. The $[(\mu\text{-pdt})Fe_2(CO)_5(CN)]^-$ anion "intermediate" was isolated as its Na^+ salt from the $Na^+[N(SiMe_3)_2]^-$ reaction, whereas the potential intermediate in the kinetic study is the Et_4N^+ salt. Thus, the overall reaction of eq 1 was monitored (by UV−vis) at 30 °C in the absence and presence of additives. (Specific data are given in the Supporting Information.) Twenty-fold excesses of $K^+PF_6^-$ to $(\mu\text{-pdt})Fe_2(CO)_6$ produced no differences in the rates of reaction. Other control experiments included the deliberate addition of water (from 200 to 1000-fold excesses to the $(\mu\text{-pdt})Fe_2(CO)_6$ reagent), acid as HCl (1:1 and 5:1 molar excesses) and base, added as Et_3N (up to 10-fold excess). In only one case was there a significant effect on the rate of reaction, and that was in the presence of large (1000-fold) excesses of water. In this case the reaction rate was significantly increased, and a different product was obtained which has not been characterized.

Table 4. Temperature Dependence of Reaction of $[Et_4N^+][CN^-]$ with $(\mu\text{-pdt})Fe_2(CO)_6$, $[Na^+][(\mu\text{-pdt})Fe_2(CO)_5(CN)^-]$, and with $(\mu\text{-}o\text{-xyldt})Fe_2(CO)_6$

compound	T, °C	(10^3) k_2, M^{-1} s^{-1}	activation parameters[d]
$(\mu\text{-pdt})Fe_2(CO)_6$[a]			
	21.5	104	$E_a = 63$ kJ/mol
	11.5	59.5	$\Delta H^‡ = 62$ kJ/mol (±8)
	1.5	20.1	$\Delta S^‡ = -66$ J/mol K (±28)
	−7.5	6.09	
$[Na^+][(\mu\text{-pdt})Fe_2(CO)_5(CN)^-]$[b]			
	23	73.1	$E_a = 36$ kJ/mol
	21	141	$\Delta H^‡ = 34$ kJ/mol (±4)
	10	65.3	$\Delta S^‡ = -164.4$ J/mol K (±14)
	1.5	32.3	
	1	34.7	
	−7.5	20.5	
	−7.5	18.6	
$(\mu\text{-}o\text{-xyldt})Fe_2(CO)_6$[c]			
	24	470	$E_a = 29$ kJ/mol
	9.5	226	$\Delta H^‡ = 26$ kJ/mol (±2)
	0	154	$\Delta S^‡ = -185$ J/mol (±8)
	−8	116	
$[Et_4N^+][(\mu\text{-}o\text{-xyldt})Fe_2(CO)_5(CN)^-]$[c]			
	24	152	$E_a = 34$ kJ/mol
	9.5	48.3	$\Delta H^‡ = 32$ kJ/mol (±11)
	−8	27.6	$\Delta S^‡ = -178$ J/mol K (±40)

[a] $[Fe_2] = 0.00766$ M; $[CN^-] = 0.137$ M. [b] $[Fe_2] \approx 0.008$ M; $[CN^-] = 0.148$ M. [c] $[Fe_2] \approx 0.00687$ M; $[CN^-] = 0.0687$ M. [d] Errors in activation parameters reported at 95% confidence.

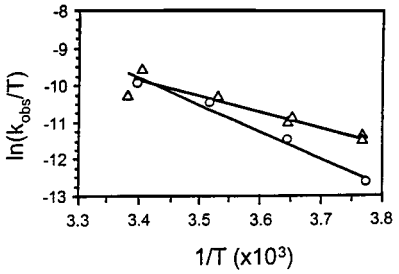

Figure 8. Eyring plot for the formation of $(\mu\text{-pdt})Fe_2(CO)_4(CN)_2^{2-}$ from $(\mu\text{-pdt})Fe_2(CO)_6$ (△) and $(\mu\text{-pdt})Fe_2(CO)_5(CN)^-$ (○).

Temperature Dependence of Reactions of $(\mu\text{-pdt})Fe_2(CO)_6$ and $(\mu\text{-pdt})Fe_2(CO)_5(CN)^-$ with CN^-. The temperature-dependence of rate constants for each of the above reactions, formation of the $(\mu\text{-pdt})Fe_2(CO)_4(CN)_2^{2-}$ complex dianion starting from the $(\mu\text{-pdt})Fe_2(CO)_6$ and from the $[(\mu\text{-pdt})Fe_2(CO)_5(CN)]^-$ complex, are given in Table 4 and presented graphically as an Eyring plot, Figure 8. Table 4 lists calculated values for enthalpy and entropy of activation as well as the E_{act} derived from Arrhenius plots. Consistent with the second-order rate expressions, small to moderate values of $\Delta H^‡$ and large negative values for $\Delta S^‡$ suggest an associative or I_a mechanism. The more negative $\Delta S^‡$ of the reaction described by eq 3, is offset by a $\Delta H^‡$ that is about half the value of that described by eq 1.

Effect of Dithiolate Bridges on CN^-/CO Exchange into $(\mu\text{-SRS})Fe_2(CO)_6$. The kinetic monitor of cyanide substitution of $(\mu\text{-}SCH_2CH_2S)Fe_2(CO)_6$ is very similar to that of the $(\mu\text{-}SCH_2CH_2CH_2S)Fe_2(CO)_6$ complex, that is in both, the dicyano final product is formed with no clear evidence of a monocyano intermediate. Conversely, the first cyanide substitution is not

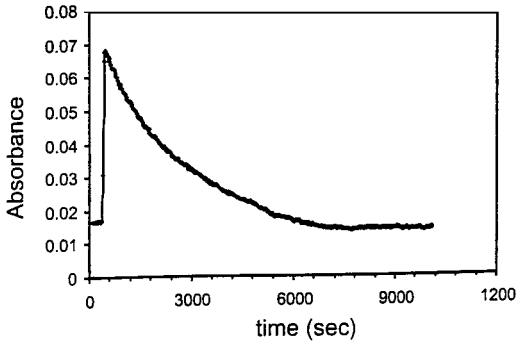

Figure 9. Time trace at 1978 cm^{-1} as (μ-$SCH_2C_6H_4CH_2S$)$Fe_2(CO)_6$ undergoes CO/CN^- exchange.

rate-limiting for the xylene-linked dithiolate complex. Infrared bands for the reactant (μ-$SCH_2C_6H_4CH_2S$)$Fe_2(CO)_6$ rapidly disappear with concomitant buildup of intermediate bands which then disappear as the dicyano product is formed. Unfortunately, the UV/vis kinetic monitor, apart from showing a very rapid disappearance of the reactant 330 nm absorbance, does not permit resolution of intermediate and product bands.

The intermediate IR bands are consistent with the (μ-*o*-xyldt)-$Fe_2(CO)_5(CN)^-$ prepared by the $N(SiMe_3)_2^-$ route (see Experimental Section); they include a prominent band at 1978 cm^{-1} whose time trace is shown in Figure 9. The rapid rate of appearance of this band permits very few data points for ln Abs versus *T* plots. Nevertheless, combined data from 12 different kinetic runs with different CN^- concentrations and temperatures were used to obtain k_2 values, Tables 1 and 4. The second-order rate constant for the initial CN^-/CO exchange in (μ-*o*-xyldt)$Fe_2(CO)_6$, k_2 in eq 2, is ~30 times greater than those of the aliphatic dithiolates. The subsequent CN^-/CO exchange yields a rate constant, k_2', closer in magnitude to the observed k_2' values of the aliphatic dithiolates, eq 4. (That is, the second-order rate constant for the second CN^-/CO exchange which was determined on the monocyano μ-pdt complex isolated from the silylamide reaction matches the second-order rate constant for the second CN^-/CO exchange in the (μ-*o*-xyldt)$Fe_2(CO)_5(CN)^-$ complex which was generated in situ and en route to the dicyano product.)

The activation energy barrier for the CN^-/CO exchange in (μ-*o*-xyldt)$Fe_2(CO)_5(CN)^-$ producing (μ-*o*-xyldt)$Fe_2(CO)_4(CN)_2^{2-}$ is similar to that of the reaction of (μ-pdt)$Fe_2(CO)_5(CN)^-$ with a second CN^-, Table 4; $\Delta H^{\ddagger}$ values are ~30 kJ/mol, and large and negative $\Delta S^{\ddagger}$ values are obtained.

^{1}H and ^{13}C NMR studies. The 22 °C ^{1}H NMR spectrum of (μ-*o*-xyldt)$Fe_2(CO)_6$ in C_6D_6 shows nonequivalent hydrogens of the methylene units in the form of two doublets positioned at 2.51 and 3.21 ppm with a J_{AB} of 13.2 Hz, Figure 10. The protons of the arene are also resolved into two resonances in the range of 6.4−6.8 ppm. An increase of temperature to +75 °C resulted in no change of pattern; the μ-*o*-xylyl group is fixed in the position observed in the solid-state structure. Likewise, the (μ-edt)$Fe_2(CO)_6$ compound, whose methylene protons are equivalent, displays a single, temperature-invariant signal in the ^{1}H NMR at 2.6 ppm.

In contrast, VT ^{1}H NMR spectra of solutions of (μ-pdt)$Fe_2(CO)_6$ display pattern changes as shown in Figure 11a. At −80 °C, four doublets represent the slow-exchange region and may be interpreted according to the solid-state structure of (μ-pdt)-$Fe_2(CO)_6$. The stick figures demonstrate that Fe_1 and Fe_2 define fused iron−dithiocyclohexane rings in the boat and chair configurations, respectively. The low-temperature spectrum shows the nonequivalency of axial and equatorial hydrogen

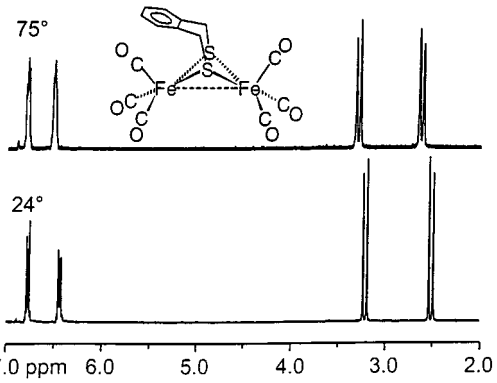

Figure 10. Ambient (24 °C) and 75 °C ^{1}H NMR spectra of (μ-$SCH_2C_6H_4CH_2S$)$Fe_2(CO)_6$ in benzene-d_6.

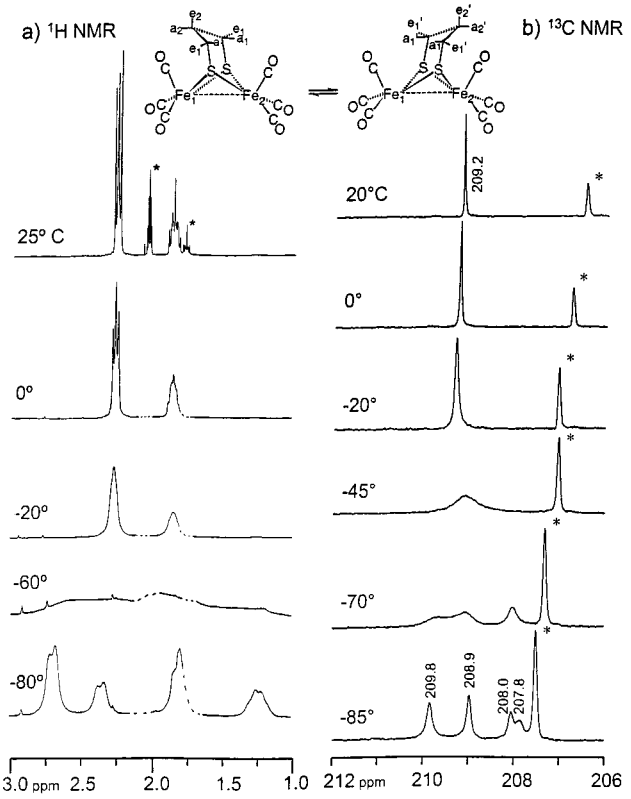

Figure 11. (a) Variable-temperature ^{1}H NMR of (μ-pdt)$Fe_2(CO)_6$ in acetone-d_6. *Solvent and impurities shown in 25 °C spectrum and then represented in remaining spectra by dotted line. (b) Low-field (CO region) ^{13}C NMR of (μ-pdt)$Fe_2(CO)_6$ at various temperatures; asterisks indicate solvent resonance, acetone-d_6.

atoms. Hydrogen atoms at the a_1 and e_1 positions are assigned to the resonances at ~1.8 and 2.7 ppm, and are doublets due to geminal $J_{a_1e_1}$ coupling of 12.0 Hz.

The other two resonances, at 1.2 and 2.3 ppm, are assigned to hydrogens of the bridgehead methylene units and also have $J_{a_2e_2}$ of 12.0 Hz. As the temperature is raised to −60 °C, coalescence occurs, and by −20 °C, the a_1e_1 hydrogens are seen as one broad resonance as are the a_2e_2 hydrogens. Upon further warming to 25 °C the lower-field resonance, centered at 2.26 ppm, resolves into three peaks, resulting from overlap of doublets. Similarly, the complex resonance centered at 1.85 ppm results from an overlapping triplet of triplets.

^{13}C NMR spectra were measured on samples isotopically enriched by photolysis of the bimetallic compounds in the presence of ^{13}C-labeled carbon monoxide. (Without photolysis, ^{13}CO exchange is slow, requiring weeks under ambient condi-

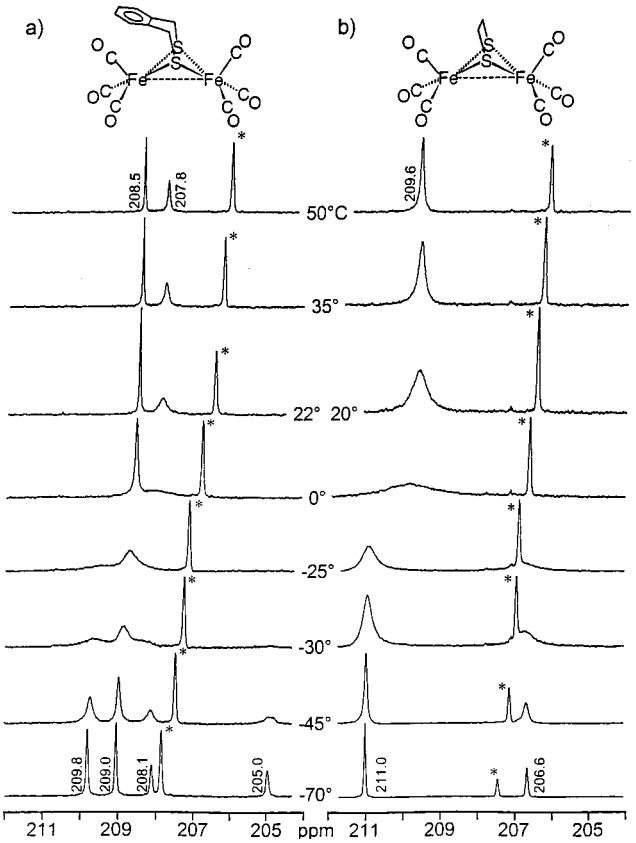

Figure 12. Low-field ^{13}C NMR at various temperatures show carbonyl resonances of (a) (*o*-xyl)$Fe_2(CO)_6$ and (b) (μ-edt)$Fe_2(CO)_6$. Solvent resonance, acetone-d_6, indicated by asterisks.

tions. Thus, the possibility of intermolecular CO site exchange is ruled out in the fluxional processes that are described below.) Figure 12a displays a selection of the variable temperature ^{13}C NMR spectra for the (μ-*o*-xyldt)$Fe_2(CO)_6$ compound. At + 50 °C, two resonances are seen; the one at lower field, 208.5 ppm, is sharper than the other at 207.8 ppm. The latter resonance broadens more rapidly than that at 208.5 ppm and coalesces into the baseline by 0 °C, while the sharper resonance never completely loses its definition. Nevertheless by −30 to −45 °C new resonances appear, one of which is shifted beyond the solvent peak. At −70 °C, four resonances are apparent, positioned at 209.8, 209.0, 208.1, and 205.0 ppm. The lower-field resonances are about double the intensity of the other two and are assigned to the basal CO's of square pyramidal (neglecting the Fe- -Fe bond) $S_2Fe(CO)_3$. The asymmetry of the molecule is a result of the stereochemical rigidity of the *o*-xylyl dithiolate group, yielding one $Fe(CO)_3$ terminus under the influence of the arene group; the other is unencumbered.

The assignment of individual ^{13}CO resonances to discrete $Fe(CO)_3$ units at the low-temperature limit of (μ-*o*-xyldt)$Fe_2(CO)_6$ benefits from spectra measured on the (μ-edt)$Fe_2(CO)_6$ complex. Here, Figure 12b, a singlet at 209.6 ppm is seen at +50 °C which broadens and reappears as two singlets by −30 °C; at −70 °C the low-temperature limit finds two sharp resonances. The one of less intensity is shifted to a higher-field position than that of the solvent, 206.8 ppm, while the other is at 211.0 ppm.

Since the $Fe(CO)_3$ units of (μ-edt)$Fe_2(CO)_6$ have no possibility of CO/π-arene interaction, we assume that the behavior of the "free" $Fe(CO)_3$ unit of (μ-*o*-xyldt)$Fe_2(CO)_6$ should be most like (μ-edt)$Fe_2(CO)_6$. In fact, the broader of the two ^{13}C resonances of (μ-*o*-xyldt)$Fe_2(CO)_6$ at +50 °C shows a line-shape

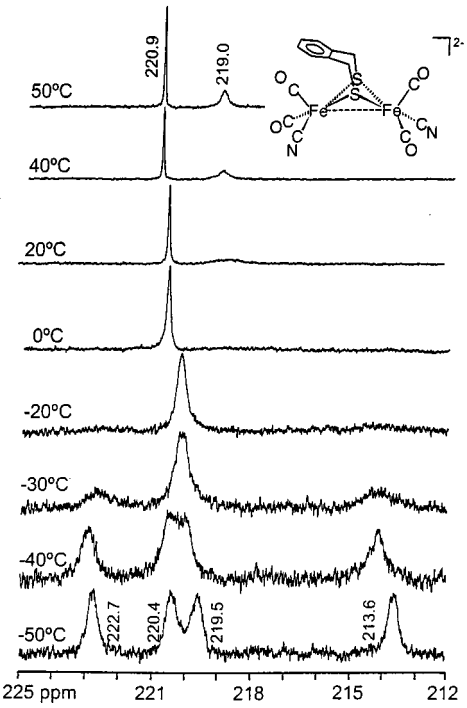

Figure 13. Carbonyl resonances of (μ-*o*-xyl)$Fe_2(CO)_4(CN)_2^{2-}$ at various temperatures. Solvent resonance, acetone-d_6, indicated by asterisks.

dependence on temperature that is practically identical to that observed for the $Fe(CO)_3$ units of (μ-edt)$Fe_2(CO)_6$ and splits into two bands separated by ~4 ppm. Thus, the assignment of the −70 °C, or slow-exchange region, spectrum of (μ-*o*-xyldt)-$Fe_2(CO)_6$ is as follows: The 209.8 and 205.1 ppm resonances arise, respectively, from the basal and apical CO's of the unencumbered $Fe(CO)_3$ unit. The closer spaced resonances at 209.0 and 208.1 ppm are for the $Fe(CO)_3$ unit in close proximity to the *o*-xylene ring.

This anisotropy is also observed in the ^{13}C NMR spectrum of the dianionic (μ-*o*-xyldt)$Fe_2(CO)_4(CN)_2^{2-}$ complex, Figure 13. As the temperature is raised, the two bands separated by 9 ppm (222.7 and 213.6 ppm) merge into one as do the two separated by only 0.9 ppm (220.4 and 219.5 ppm).

Activation barriers for the $(CO)_{ap}/(CO)_{ba}$ site permutations may be estimated from the exchange rate constant, at coalescence ($k_r = (\pi)/\ 2$; and $\Delta G^{\ddagger} = RT\ \ln(k_B T/k_r h)$),[29] and from Arrhenius plots of rate constants determined from line widths in the slow-exchange region of the spectrum,[30] or from rate constants derived from spectral simulations by dynamic NMR computer programs. By the first method, for the two identical sites of (μ-edt)$Fe_2(CO)_6$, $\Delta G^{\ddagger}$ is found to be 50.7 kJ/mol, and the analogous or sterically unencumbered $Fe(CO)_3$ terminus of (μ-*o*-xyldt)$Fe_2(CO)_6$ is similarly 51.5 kJ/mol. The single-point (coalescence) activation energy computation shows a slight difference for the $(CO)_{ap}/(CO)_{ba}$ site exchange under the influence of the xylyl ring; it is 49.7 kJ/mol.

The other two methods for determining rate constants and their temperature dependence showed a greater discrepancy in E_{act} for the two $Fe(CO)_3$ rotors of the (μ-*o*-xyldt)$Fe_2(CO)_6$ molecule, with the *o*-xylyl-encumbered $Fe(CO)_3$ terminus having the smaller value in each case: By line width analysis in the slow-exchange region, 37.5 and 27.8 kJ/mol, while spectral

(29) Kessler, H. *Angew. Chem., Int. Ed. Engl.* **1970**, *9*, 219.
(30) Drago, R. S. *Physical Methods for Chemists*, 2nd ed.; Saunders College Publishing: Ft. Worth, TX, 1992; p 291−295.

simulation yielded 34.5 and 23.0 kJ/mol as E_{act} for the unencumbered and encumbered $Fe(CO)_3$ termini, respectively.

Activation energies derived from analyses of dynamic NMR are notoriously inaccurate. Within the experimental error of the approaches, all of the above derived $\Delta G^{\ddagger}$ values are probably indistinguishable. We accept with a degree of assurance that the activation barriers are relatively small (and similar to those determined earlier on compounds in this class, 40−63 kJ/mol).[31] Furthermore, the asymmetry imposed on the (μ-*o*-xyldt)$Fe_2(CO)_6$ molecule by the rigidity of the bent-over *o*-xylyl ring somewhat lowers the rotation barrier of that $Fe(CO)_3$ closest to the ring.

It is noteworthy that at the high-temperature limit of our experiments (+50 °C on a 300 MHz NMR instrument), CO exchange between the $Fe(CO)_3$ units of (μ-*o*-xyldt)$Fe_2(CO)_6$ does not occur. This is consistent with other studies of analogous asymmetrically substituted diiron systems.[31] In addition, within the (μ-*o*-xyldt)$Fe_2(CO)_6$ molecule, the $Fe(CO)_3$ unit encumbered by the close proximity of the xylyl arene group experiences less magnetic anisotropy, that is, shows a smaller splitting of the ^{13}C signals for apical and basal CO groups, than does the unencumbered or "free" $Fe(CO)_3$ unit. The effect of the hovering arene diminishes the inherent anisotropy for the $(CO)_{ap}/(CO)_{ba}$ sites and shifts the apical CO downfield. There is, however, a small and positive effect of this fixed arene on the $Fe(CO)_3$ rotation rate. This was unexpected, as the close proximity of sterically bulky groups typically impede molecular motion. A possible explanation has been sought from theory, vide infra.

Shown in Figure 11b are the VT ^{13}C NMR spectra of (μ-pdt)$Fe_2(CO)_6$ in CH_3CN solution. The sharp singlet observed at 20 °C broadens, coalesces at ∼−50 °C, and becomes four distinct resonances in the −70 to −85 °C range. The barrier to CO site exchange was calculated to be 43.5 kJ/mol. The VT ^1H NMR spectra also show configurational mobility in the iron−dithiacyclohexane ring which is frozen out between −20 and −60 °C. This is in contrast to the (μ-*o*-xylyl)$Fe_2(CO)_6$ molecule where the VT ^1H NMR shows the S-to-S hydrocarbon is fixed even at high temperatures. The difference in mobility of the iron−dithiacyclohexane ring as compared to the iron−dithiacycloheptane ring in the (*o*-xylyl)Fe_2 unit is accounted for by the rigidity induced by the sp^2 carbons connecting the arene group into the latter ring. Nevertheless, at low temperatures where the pdt-Fe ring is locked into place, there is asymmetry or magnetic anisotropy in the $Fe(CO)_3$ termini, similarly to the *o*-xyldt complex. While one expects the chemical shift difference in $(CO)_{ap}$ versus $(CO)_{ba}$ sites to be similar to those in (μ-edt)$Fe_2(CO)_6$, they are considerably, and inexplicably, smaller.

Theoretical Results. To gain insight into a possible connection between the intramolecular complex mobility and the intermolecular ligand-exchange process, a theoretical approach to the possible transition states or intermediates appropriate to the site-exchange process of the (μ-*o*-xyldt)$Fe_2(CO)_6$ compound has been initiated. A full disclosure and in depth discussion of the results from density functional theory computations will be presented elsewhere.[32]

The molecule represented in Figure 14, structure **A**, is the ground-state, geometry-optimized structure of (μ-*o*-xyldt)$Fe_2(CO)_6$; the two $Fe(CO)_3$ units are eclipsed as is observed in the crystal structure. Structure **B** is the geometry-optimized structure with the $Fe(CO)_3$ terminus which is in close proximity to the arene rotated by 60° relative to the adjacent $Fe(CO)_3$ unit, creating a staggered projection. Structure **C** is also a staggered form but with the opposite or "free" end rotated. Notably, the geometry of the optimized structures, where one $Fe(CO)_3$ unit has been rotated, distorts from the simple staggered form that was the inputted structure to an inverted square pyramidal geometry. Frequency calculations determined that structures **B** and **C** are transition states.[33] The overall energies are listed underneath each structure and show structure **C** to be higher in energy than is structure **B**. That is, the smaller energy difference is between the ground state, structure **A**, and transition state, **B**, and, as such, represents the rotation with the smaller activation energy barrier for the $Fe(CO)_3$ rotor. While the difference of 8 kJ/mol is higher than our admittedly precarious experimental results from NMR, it is, nevertheless, in the correct direction.

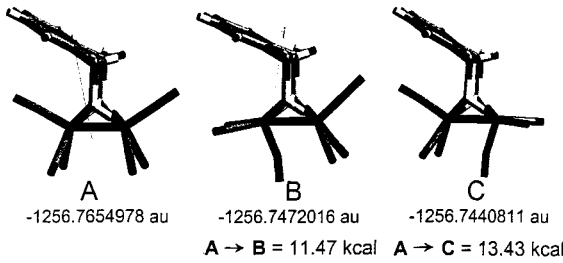

Figure 14. Geometry-optimized structures of (μ-*o*-xyldt)$Fe_2(CO)_6$, (A) is ground state; (B) and (C) have one $Fe(CO)_3$ unit rotated by 60°. MSI Cerius graphical interface was used.

A qualitative view of these molecular machinations lies in the repulsive interaction of arene with apical Fe−CO which raises the ground state of that $Fe(CO)_3$ unit in structure **A** relative to the transition state represented by structure **B**. Relief of that steric strain occurs as a CO moves off center of the arene, structure **B**, actually allowing the arene ring to relax down as the pseudo-square-pyramid of $S_2Fe(CO)_3$ is effectively inverted. The unencumbered $Fe(CO)_3$ unit (or units, as seen in (μ-edt)$Fe_2(CO)_6$) experiences none of this ground-state destabilization and transition-state steric relief. In fact, the full analysis of the optimized structures finds that rotation of the unencumbered $Fe(CO)_3$ unit results in an even closer approach of apical CO to arene group in the encumbered unit. That the close approach, 3.12 Å for the average CO vector to C_6-plane distance in the solid-state crystal structure is repulsive in nature is supported by the fact that vibrational analysis of CO/benzene van der Waals clusters, as produced in supersonic molecular jets and probed by two-laser, time-of-flight mass spectrometry, finds a longer distance of 3.24 Å.[34] Furthermore the expected van der Waals contact distance as determined from ab initio calculations is ∼3.5 Å.

The HOMO of the ground-state structure of such dinuclear complexes is the Fe- -Fe bond.[35] The result of twisting the $Fe(CO)_3$ unit by 60°, that is, toward a trigonal prism arrangement of a hexacoordinate species, is nonoptimal orbital overlap for the Fe- -Fe bond. This partial disruption of the bond is reflected in the Mulliken charge redistribution from symmetrical Fe(−1.04)Fe(−1.05) to Fe(−0.84)Fe(−1.22). Thus the E_{act} barrier for CO site exchange reflects loss of Fe- -Fe bond character and a shift of the electron density toward the $Fe(CO)_3$

(31) (a) Flood, T. C.; DiSanti, F. J.; Campbell, K. D. *Inorg. Chem.* **1978**, *6*, 1643. (b) Adams, R. D.; Cotton, F. A.; Cullen, W. R.; Hunter, D. L.; Mihichuk, L. *Inorg. Chem.* **1975**, *14*, 1395.

(32) Lyon, E. J.; Thomson, L. M.; Hall, M. B.; Darensbourg, M. Y. Manuscript in preparation.

(33) Jensen, F. *Introduction to Computational Chemistry*; J. Wiley & Sons: New York, 1999; Chapter 14.

(34) Nowak, R.; Menapace, J. A.; Bernstein, E. R. *J. Chem. Phys.* **1988**, *89*, 1309.

(35) Teo, B. K.; Hall, M. B.; Fenske, R. F.; Dahl, L. F. *Inorg. Chem.* **1975**, *14*, 3103.

unit that is not rotated. Concomitantly, there develops a semi-bridging CO group, to access the polarized electron density, as well as an open site on the rotated $Fe(CO)_3$ unit. In structure **B**, this open site is underneath the arene; in structure **C**, it is more available.

Summary and Comments

The above series of bidentate bridging dithiolates in (μ-SRS)-$Fe_2(CO)_6$ are discussed here, according to our view of the (μ-SRS)Fe_2 unit as fused-iron−ithiocycloalkane rings. The analogy with cycloalkanes is congruous with the Seyferth et al. comparison of the $S_2Fe_2(CO)_6$ unit as an organic disulfide[36] and suggests conformational preferences, the result of which is the basis of several conclusions, highlighted below.

- As reported by ν(CO) values, differences in S-donor ability are negligible for the three dithiolate ligands in the series. They render the $Fe(CO)_3$ units in nearly identical electronic environments, consistent with metric parameters from molecular structures.
- Intramolecular dynamic processes typify both the (μ-SRS)-Fe_2 fused ring unit as well as the iron diatomic ligand sites.
- Conformational preferences in the (μ-SRS)Fe_2 fused ring unit induce asymmetry to the $Fe(CO)_3$ termini when the rings are fixed. This asymmetry is strictly the result of a steric difference through space. It produces a close contact of arene and CO in the case of the (μ-*o*-xyldt)$Fe_2(CO)_6$ compound, inducing an obvious magnetic anisotropy as expressed by ^{13}C NMR shifts or positions. A lesser effect is noted for the (μ-pdt)$Fe_2(CO)_6$ compound.
- The dynamic processes of the $Fe_2(CO)_6$ portion are centered in apical/basal CO site exchanges through a turnstile rotation or trigonal twist at discrete $S_2Fe(CO)_3$ units, components of pseudo-square-pyramids (neglecting the Fe- -Fe bond as a sixth "ligand" position), or pseudo-octahedra (the Fe- -Fe bond occupying the sixth site).
- Cyanide readily exchanges with carbonyl ligands by associative processes in both the first CO/CN^- exchange to produce a monocyano anion as well as in the second exchange, ultimately producing a stable dicyano dianion which has one CN^- on each iron. The isolated monocyano intermediates are established to be thermodynamically less stable than the dicyano, dianionic products.
- The (μ-pdt)$Fe_2(CO)_6$ compound, fluxional in both the iron−dithiocyclohexane ring as well as the $Fe(CO)_3$ units, has a nearly identical CN^-/CO substitution reaction profile as the nonsterically encumbered and less fluxional (μ-edt)$Fe_2(CO)_6$ compound. The rate-limiting step for CN^-/CO substitution is addition of the first cyanide, rather than the second.
- The (μ-*o*-xyldt)$Fe_2(CO)_6$ compound, rigid in the (μ-SRS)-Fe_2 rings at NMR accessible temperatures and with intramolecular CO permutations distinct for the two $Fe(CO)_3$, shows a CN^-/CO reaction profile that is different from the other two members of the series. It has the fastest rate in the first CN^-/CO substitution, and the rate-limiting step is addition of the second cyanide, rather than the first. Nevertheless the overall rates and activation barriers are comparable.

We propose that the transition states or intermediates of intramolecular fluxional processes relate to the intermolecular CN^-/CO-exchange processes in the following way. The overall molecular architecture and subtle factors which influence the coordination sphere intramolecular rearrangements are also required in the ligand-substitution reaction. In particular, the theoretical calculations of transition states for the *intra*molecular $Fe(CO)_3$ rotor processes, structures **B** and **C**, serve as indicators for the molecular rearrangements that must occur concurrently as CN^- gains access to the iron in the *inter*molecular CN^- associative or nucleophilic addition path. That the facile structural rearrangements occur along a soft reaction profile, with shallow minima, is consistent with the low barriers to CN^-/CO exchange. *That a polarization of the electron density in the iron−iron bond and a bridging CO develops is expected as a viable intermediate preceding CO loss.* Most importantly, the presence of the anionic CN^- ligand would better stabilize a bridging CO and explain the ease of the second CN^-/CO exchange.

As to why the two anionic reagents, CN^- and $(Me_3Si)_2N^-$, both of which react via bimolecular mechanisms with metal carbonyls, respond so differently to the intermediate (μ-SRS)-$Fe_2(CO)_5(CN)^-$ anion must lie in the site preference for nucleophilic attack. Cyanide reacts at the iron, directly implementing CO/CN^- exchange. However, the CO conversion to CN^- via the $(Me_3Si)_2N^-$ reagent requires nucleophilic attack at CO carbon, involving a greater sensitivity to the charge on carbon and higher barriers to the multiple bond breaking/remaking process.

Relation to [FeFe] Hydrogenase Active Site. The impetus for this work overall was to provide insight into the presence of a similar fragment in the active site of [FeFe]H_2ase. This set of model complexes and their chemistry indicate that the dithiolate bridge firmly binds two low-valent iron centers together, permitting chemistry to occur on an intact binuclear complex. It suggests that low-valent iron chemistry (oxidation states of +1 and +2, rather than +2/+3 as previously presumed) could prevail within the active site.[37] Recent binding studies of exogenous CO and ^{13}CO further support the presence of low-valent Fe(I) in the active site.[38] Electron density in the iron (I) centers is polarizable, responding even to geometrical shifts in the iron diatomic site, thus facilitating charge distribution in a redox active site. Overall there is considerable mobility possible within the coordination sphere, suggesting ease of substrate binding and release. An attractive conclusion from the computations is that the similarity between the [FeFe]H_2ase active site and the optimized structure of the $Fe(CO)_3$ rotated state, signifies that the enzyme has trapped, via H-bonding interactions to cyanide, a higher-energy configuration in the active site.

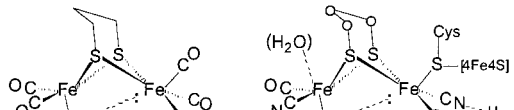

Nature's selection of an organic dithiolate rather than two cysteines as the bridging thiolates for this dinuclear unit is fascinating. Vibrational spectroscopic studies of analogous alkanethiolates (μ-SRS)$Fe_2(CO)_6$ versus (μ-SR)$_2Fe_2(CO)_6$ find minimal differences in electronic effects transmitted to the iron as reported by ν(CO). Hence, the advantage of a bidentate-bridging dithiolate over two monodentate ligands is not electronic but must lie in the structural or stability attributes provided by the bidentate-bridging ligand. In that regard, should the unit be preassembled and imported into the apoprotein, organic

(36) Seyferth, D.; Henderson, R. S. *J. Organomet. Chem.* **1981**, *218*, C34.

(37) Popescu, C. V.; Münck, E. *J. Am. Chem. Soc.* **1999**, *121*, 7877.

(38) De Lacey, A. L.; Stadler, C.; Cavazza, C.; Hatchikian, E. C.; Fernandez, V. M. *J. Am. Chem. Soc.* **2000**, *122*, 11232.

linked sulfides are attractive both for stability and for sulfide protection during access into the protein.

The requirement of a three-atom linker in the S-to-S bridge provides even more intellectual stimulus. If the three atoms are all carbon, the propanedithiolate bridge might be serving as a molecular recognition unit, providing a steric interaction that aids in anchoring the active site. Should the central atom be a NH functionality, whose possibility has been noted by the protein crystallographers and verified as reasonable by theory,[3,39] it would be ideally oriented to shuttle protons in and out of the active site via the adjacent cysteine 178 (in DdH).[3] That is, a built-in proximal base to remove H^+ from an (η^2-H_2)Fe complex, or to add H^+ to reduced iron producing H−Fe, adequately explains the H_2 heterolytic activation process. Our work has shown that the three light atoms offer a hinge motion that can facilitate the proton transfer from metal to the cysteine proton acceptor or, if needed, completely flip the base away from the active site.

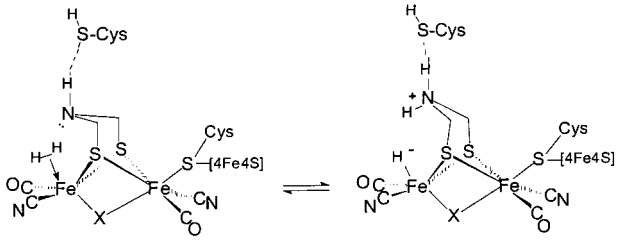

Clearly an understanding of the bioassembly process of the [FeFe]H_2ase active site is critical to further development of the role of such organometallic chemistry in nature. Advances in this research arena were recently reported in the form of identification of carbamoyl phosphate as the likely source of the diatomic CO and CN ligands in the [NiFe]H_2ase.[40] In view of the rich organic chemistry that occurs at bridging sulfide sites of low-valent iron dimers,[10,36] we conjecture that the -$(CH_2)_3$-dithiolate, the -(CH_2NHCH_2)-dithiolate, or whatever sulfide or sulfide derivative bridges the two iron center, could be among a plethora of iron−sulfur-mediated transformations.

Acknowledgment. We acknowledge financial support from the National Science Foundation (CHE-9812355 for this work, CHE 85-13273 for the X-ray diffractometer and crystallographic computing system) and contributions from the R. A. Welch Foundation. A National Institutes of Health Training Grant 5-T32-GM08532 (Graduate Training in Biological Chemistry) provided support for E. J. L. We are obliged to the D. J. Darensbourg group for use of their ReactIR, and we are grateful for the technical assistances of Dr. Brian Frost, Jason Smee, and Lisa Thomson. Discussions with Drs. D. J. Darensbourg, F. Gabbai, M.B. Hall, D. Singleton, and D. Russell are much appreciated.

Supporting Information Available: Molecular structure and X-ray crystallographic tables for (μ-xyldt)$Fe_2(CO)_6$, rate constants determined using UV−vis spectroscopy and control experiments (PDF). This material is available free of charge via the Internet at http://pubs.acs.org.

JA003147Z

(39) Fan, H.-J.; Hall, M. B. *J. Am. Chem. Soc.* **2001**, *123*, in press.

(40) Paschos, A.; Glass, R. S.; Böck, A. *FEBS Letters* **2001**, *488*, 9.